A Real-Time In Situ Wafer Temperature Measurement System Based on Fiber Bragg Grating Array

Yuhao Feng, Jingjing Peng, Tao Wu, Fei Xing, and Ting Sun

***Abstract*—Temperature is an essential parameter in the silicon-based micro electro mechanical system (MEMS) fabrication process, and the uneven temperature distribution on a wafer surface could significantly impact the whole fabrication process. This research aims to observe the wire bonding system's heating process from 30 °C to 110 °C. A temperature sensor network consisting of multiple fiber Bragg gratings (FBGs) is proposed for real-time wafer surface temperature monitoring. The temperature points measured by FBG sensors are used to construct the temperature distribution of the entire wafer surface, enabling tracking of the hotspots during the heating processes. Additionally, a comparative analysis of the FBG sensor network's results was conducted using those gathered by infrared thermal imager and thermocouple (TC) sensors. The results indicate the existence of a temperature gradient along the wafer's surface in the radial direction, with a maximum temperature difference of 11.94 °C and the temperature distribution taking the shape of approximate concentric circles. The FBG sensor network offers a clear and intuitive illustration of the wafer's surface temperature distribution during heating, providing real-time responses. Therefore, the proposed temperature measurement network based on FBG sensors can effectively monitor the temperature defects on the wafer surface during the MEMS process.**

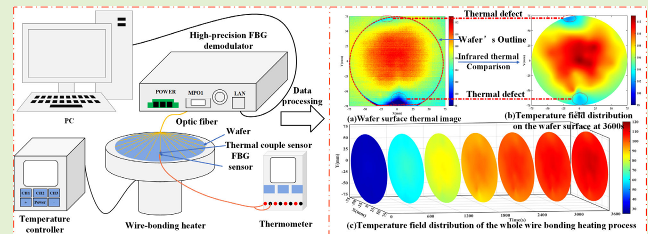

***Index Terms*— Fiber Bragg grating (FBG), in situ wafer temperature measurement, temperature field reconstruction.**

I. Introduction

WAFER temperature is a crucial factor in silicon-based micro electro mechanical system (MEMS) manufacturing, and temperature measurement errors are relatively common in many processes. Even slight temperature variations and inhomogeneity in the MEMS fabrication process can impact the final chip performance. For instance, in the chemical vapor deposition (CVD) process, precise temperature control is related to the deposition quality of the thin film [1]. In the physical vapor deposition (PVD) process [2], the adhesion between the film and the substrate depends mainly on the process temperature. In the atomic layer deposition (ALD) process [3], temperature inconsistencies can significantly impact the conformality of the deposited film. Moreover, in the rapid thermal process (RTP), ensuring the repeatability and uniformity of the temperature effectively reduces the wafer warpage and slippage to improve product yield [4], [5]. In the photolithography process [6], [7], the chemical amplification resist used in the DUV photolithography process is particularly sensitive to temperature changes. In summary, the temperature affects almost the entire MEMS manufacturing process. Hence, real-time and accurate wafer temperature monitoring becomes pivotal in meeting the requirements of manufacturing high-performance MEMS chips and obtaining higher temperature control accuracy in the process equipment.

The current wafer temperature monitoring methods are mainly divided into two types: noncontact measurement and contact method. Noncontact temperature measurement methods include radiation temperature measurement [8], reflectivity temperature measurement methods [9], infrared transmission

Manuscript received 15 March 2024; revised 7 April 2024; accepted 7 April 2024. Date of publication 18 April 2024; date of current version 31 May 2024. This work was supported in part by the National Natural Science Foundation of China (NSFC) under Grant 62375022; and in part by the Optoelectronic Measurement and Intelligent Perception Zhongguancun Open Laboratory, and Space Optoelectronic Measurement and Perception Laboratory, Beijing Institute of Control Engineering under Grant LabSOMP-2022-02. The associate editor coordinating the review of this article and approving it for publication was Prof. Carlos Marques. *(Corresponding authors: Fei Xing; Ting Sun.)*

Yuhao Feng and Ting Sun are with the School of Instrument Science and Opto-Electronics Engineering, Beijing Information Science and Technology University, Beijing 100192, China (e-mail: sunting@bistu.edu.cn).

Jingjing Peng and Tao Wu are with the State Key Laboratory of Precision Measurement Technology and Instruments, Tsinghua University, Beijing 100084, China (e-mail: pengjingjing@qiyuanlab.com).

Fei Xing is with the Department of Precision Instrument, Tsinghua University, Beijing 100084, China (e-mail: xingfei@mail.tsinghua.edu.cn).

Digital Object Identifier 10.1109/JSEN.2024.3387989

© 2024 The Authors. This work is licensed under a Creative Commons Attribution-NonCommercial-NoDerivatives 4.0 License.
For more information, see https://creativecommons.org/licenses/by-nc-nd/4.0/

temperature measurement [10], refractive index and radiation combined temperature measurement [11], polarization transmission method [12], [13], interferometric temperature measurement [14], [15], infrared thermography temperature measurement [16], [17], and acoustic method [18]. The most widely used radiation temperature measurement method is based on Planck's blackbody radiation law and requires accurate measurement of the emissivity of the wafer before measurement. The latter mainly refers to the use of thermocouples (TCs) [19], [20], [21], [22], [22], reactive resistors [23], and transistors [24], [25] as temperature sensors. Multiple sensors are formed into a sensor array on the wafer surface and connected to the external temperature of the process equipment via electrical wires to obtain the 2-D temperature field distribution. However, these electrically based contact wafer temperature measurement methods have several problems, including sensitivity and baseline drift caused by Joule heating and the elimination of microroughness on the surface, requiring a constant current and voltage to be continuously applied to the sensors.

To address these issues, this study proposes using fiber Bragg gratings (FBGs) as temperature sensors arranged on the wafer surface. Although the FBG has been widely used in many temperature measurement scenarios in the following fields, such as lithium battery temperature monitoring [26], [27], [28], IGBT module temperature monitoring [29], [30], [31], and power transformer winding temperature measurement [32], [33], FBG sensors can be coated and fabricated in combination with various materials to improve their sensing performance in a particular area. For example, [34] mentions that combining FBG sensors with thermoplastic polyurethane (TPU) materials can extend the application of FBG sensors for gait-assisted wearable device instrumentation outside the clinical setting. In [35], FBG embedded in silicone rubber diaphragms was used to detect the liquid level of JET A-1 aviation fuel, and its performance was four times better than in previous studies. In [36], a pH-sensitive layer made of polyaniline (PANI) was deposited on the surface of a tapered single-mode fiber and a D-type plastic fiber to achieve a reproducible and repeatable pH sensor with insignificant temperature and ionic strength cross-sensitivity effects. Mishra et al. [37] coats the surface of optical fiber with materials such as lead, indium, copper, aluminum, and PMMA to achieve the improvement of temperature sensitivity of FBG sensors, among which PMMA has the best sensitization effect. Applying FBG sensors to wafer surface temperature measurement maximizes their benefits, such as small size, nonconductivity, resistance to electromagnetic interference, and multipoint measurement.

This article focuses on improving the coverage rate of the temperature sensor network on the wafer surface by increasing the number of sensors. To achieve this, two temperature measurement wafers (TMWs) utilizing FBGs as temperature sensors are fabricated. The linear temperature measurement wafer (LTMW) concentrates on the central temperature of the wafer, which is made up of 20 FBGs. The LTMW is easy to fabricate, but due to its small number of sensors, the wafer surface edge distribution reconstruction accuracy is poor when performing temperature field reconstruction. To improve the accuracy of temperature field reconstruction, the fan-shaped temperature measurement wafer (FTMW) was fabricated to focus on the overall surface temperature of the wafer, consisting of 54 FBGs. The wafer temperature measurement experiment platform is constructed using a wire bonding system. By utilizing the Gauss radial basis function (GRBF) algorithm, a temperature field that can respond to the spatial-temporal temperature distribution on the wafer surface is constructed. The FBG sensor network's results are compared using data gathered by infrared thermal imager and TC sensors to illustrate the validity of temperature field reconstruction. The proposed TMW system has high accuracy and can effectively respond to the temperature distribution on the wafer surface, providing valuable data for temperature control in MEMS processes.

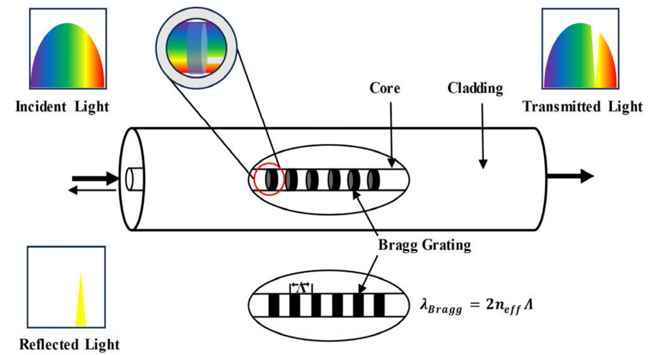

Fig. 1. Measurement principle of the FBG temperature sensor.

II. Design and Fabrication of TMW Based on FBG Array

A. Temperature Sensing Principle of FBG Sensors

As Fig. 1 shows, the FBG operates as a reflective filter inscribed in the optical fiber core through periodic perturbations of reflectivity along the fiber's length. When broadband light enters the core, only light that matches the FBG is reflected while the rest is transmitted. The reflected wavelength and the Bragg wavelength are determined by the phase-matching condition. The resonance condition can be expressed as the Bragg wavelength that satisfies the mode coupling theory

$$\lambda_{\text{Bragg}} = 2n_{\text{eff}}\Lambda \quad (1)$$

where n_{eff} is the fiber propagation mode's effective refractive index and Λ is the grating period.

The wavelength reflected by an FBG is determined by the grating period and the effective refractive index of the fiber core. FBG sensors are susceptible to environmental changes, especially in temperature fields. Due to the thermal expansion of FBG and the thermooptical effect, the grating period and effective refractive index of FBG change, leading to a shift in the center wavelength of the FBG. The amount of wavelength shift is directly proportional to the temperature change and

can be expressed as follows:

$$\frac{\Delta\lambda_{\text{Bragg}}}{\Delta T} = 2\left(\Lambda\frac{\partial n_{\text{eff}}}{\partial T} + n_{\text{eff}}\frac{\partial\Lambda}{\partial T}\right). \tag{2}$$

Substitute (1) into (2)

$$\Delta\lambda_{\text{Bragg}} = \left(\frac{1}{n_{\text{eff}}}\frac{\partial n_{\text{eff}}}{\partial T} + \frac{1}{\Lambda}\frac{\partial\Lambda}{\partial T}\right)\lambda_{\text{Bragg}}\Delta T. \tag{3}$$

The amount of Bragg wavelength change is related to the temperature change of the FBG, and the temperature-dependent change in the FBG period is thought to be much smaller than the temperature-dependent change in the effective refractive index, as ($\alpha = (1/n_{\text{eff}})(\partial n_{\text{eff}}/\partial T) \gg \xi = (1/\Lambda)(\partial\Lambda/\partial T)$). α is called the fiber thermooptical coefficient ($\approx 0.55 \times 10^{-6}$/°C), and β is called the linear coefficient of thermal expansion ($\approx 6.1 \times 10^{-6}$/°C). The relationship can finally be described as follows:

$$\Delta\lambda_{\text{Bragg}} = (\alpha + \xi)\lambda_{\text{Bragg}}\Delta T. \tag{4}$$

It can be seen that the change in the Bragg wavelength of FBG is directly linked to the variations in temperature. Moreover, it is possible to calibrate the correlation between temperature and wavelength to suit a particular FBG sensor. This enables an accurate measurement of the temperature value based on the reflected Bragg wavelength.

B. Design and Fabrication of FBG-Based TMW

This study used a single-mode fiber manufactured by Beijing SmarsTek Company, and the fiber grating array was fabricated using the traditional phase mask method [38], [39], [40]. The inner diameter of the fiber core is 80 μm, and the cladding diameter is 110 μm. The sleeve thickness is 400 μm, and the material adopts freely expanded polyimide. To satisfy the requirement of the wafer surface temperature monitoring, two types of surface-mounted fiber grating wafers were designed: linear and fan-shaped. The LTMW consists of a wafer substrate and four optical fibers. SY-40 epoxy resin is used to fix the optical fibers on the wafer surface, and five FBGs are arranged uniformly on each optical fiber to monitor the temperature in the central part of the wafer. The central wavelengths of all the FBGs are shown in Table I, and the schematic and prototype of the LTMW are demonstrated in Fig. 2(a) and (b). A serial number (i, j) represents the sensor matrix, where i represents the number of fibers in which the FBGs are located, and j represents the serial number of sensors on the same fiber where the FBG is arranged according to the central wavelength from minimum to maximum. In order to improve the temperature field reconstruction accuracy, the number of sensors arranged on the wafer surface is increased, and the coverage area of the optical fiber on the wafer surface is expanded. The illustration of the FTMW structure can be found in Fig. 3. It comprises a substrate wafer and 15 optical fibers with 54 FBG sensors. The central wavelengths of these FBGs are listed in Table II, and their serial number follows the rules mentioned above.

TABLE I
CENTRAL WAVELENGTHS OF THE FBGS ON THE LTMW

Optical fiber	FBG1 (nm)	FBG2 (nm)	FBG3 (nm)	FBG4 (nm)	FBG5 (nm)
1	1531.053	1535.001	1538.861	1543.045	1547.130
2	1531.067	1535.032	1539.068	1543.079	1546.951
3	1531.044	1535.011	1538.860	1543.015	1546.909
4	1531.060	1535.066	1538.886	1543.064	1546.954

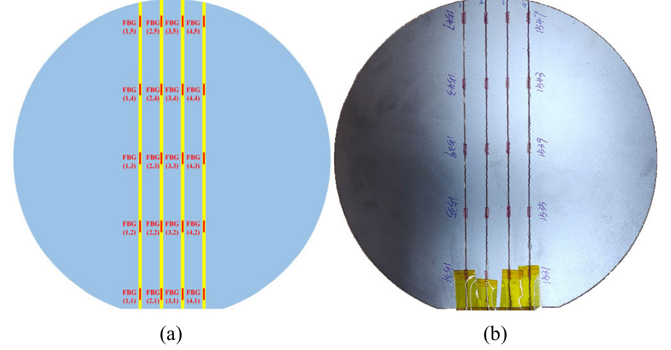

Fig. 2. Schematic of the linear-shaped FBG temperature measurement wafer. (a) Wafer with sensors' serial numbers. (b) Diagram of the prototype.

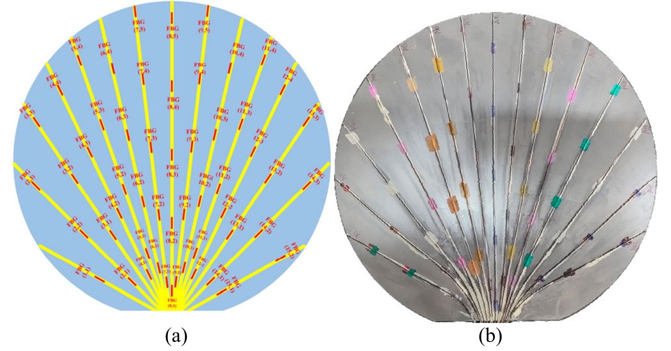

Fig. 3. Schematic of the fan-shaped FBG temperature measurement wafer. (a) Wafer with sensors' serial numbers. (b) Diagram of the prototype.

C. Calibration of FBG-Based TMW

The temperature calibration is carried out for two TMWs before the experiment to improve the measurement accuracy. The calibration platform is shown in Fig. 4, which consists of an optical spectral analyzer, a high-precision FBG demodulator, a high-precision constant-temperature water bath, and a high-precision PT100 thermometer. It is calibrated at the temperatures of 35 °C, 40 °C, 50 °C, 60 °C, 70 °C, 80 °C, and 90 °C, respectively. In Fig. 5, the central wavelength of the FBG sensor on the LTMW drifts linearly with temperature variation. It can be seen that the temperature resolution of the FBG sensors is 9.98–12.22 pm/°C. Fig. 6 shows the central wavelength shift of the FBG sensor on the FTMW. It can be seen that the temperature resolution of the FBG sensor is 9.92–10.15 pm/°C. The correlation coefficient is all greater than 0.99, and the above results demonstrate the excellent linearity of the FBG sensors on both TMWs.

TABLE II
CENTRAL WAVELENGTHS OF THE FBGS ON THE FTMW

Optical fiber	FBG1 (nm)	FBG2 (nm)	FBG3 (nm)	FBG4 (nm)	FBG5 (nm)
1	1536.156	/	/	/	/
2	1529.897	1533.064	1536.114	/	/
3	1539.040	1542.168	1545.088	/	/
4	1554.188	1557.175	1560.134	1563.163	/
5	1554.177	1557.178	1560.129	1563.024	/
6	1529.811	1533.127	1536.088	1539.354	/
7	1529.930	1533.188	1536.156	1539.179	1542.185
8	1545.028	1547.977	1551.046	1554.075	1557.042
9	1545.347	1548.129	1551.064	1554.176	1557.207
10	1542.192	1545.097	1548.113	1551.201	/
11	1542.170	1545.070	1548.101	1551.036	/
12	1530.088	1533.179	1536.144	1539.143	/
13	1539.150	1542.266	1545.174	/	/
14	1530.018	1533.163	1536.132	/	/
15	1548.299	1551.217	/	/	/

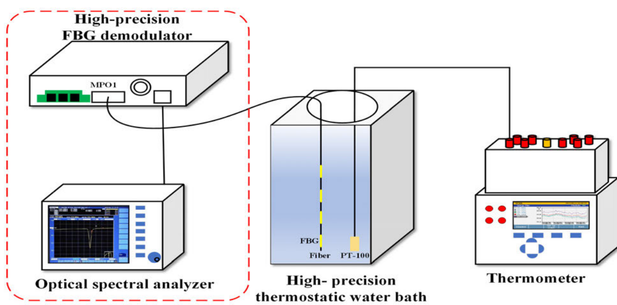

Fig. 4. Schematic of the experimental setup for fiber Bragg grating temperature sensor calibration.

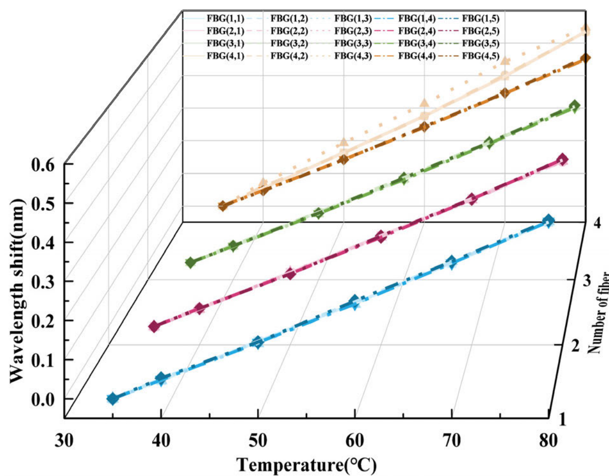

Fig. 5. Sensitivity of the FBG sensors on each optical fiber in the range of 35 °C–80 °C.

D. Construction of the Wafer Temperature Heating Monitoring Experiment Platform

A set of corresponding experimental platforms for monitoring the wafer temperature heating process is built using the wire bonding system, as shown in Fig. 7. It consists of the wire bonding machine and its heating temperature control equipment, a multichannel thermometer, TCs from Omega Engineering Inc., a FBG demodulator, TMWs, and a PC, of which the critical parameters of the equipment are shown in Table III. The heating platform provides a heating range of 30 °C–110 °C, the PC is responsible for collecting temperature data after demodulation, and the Fluke infrared thermal imager is used to measure the temperature distribution on the wafer surface at different center temperatures. The TCs are affixed next to the FBG using Kyowa CC-33A Cyanoacrylate resin glue and cured for one hour to ensure measurement accuracy. The TC is used to compare and evaluate the accuracy of the FBG measurement.

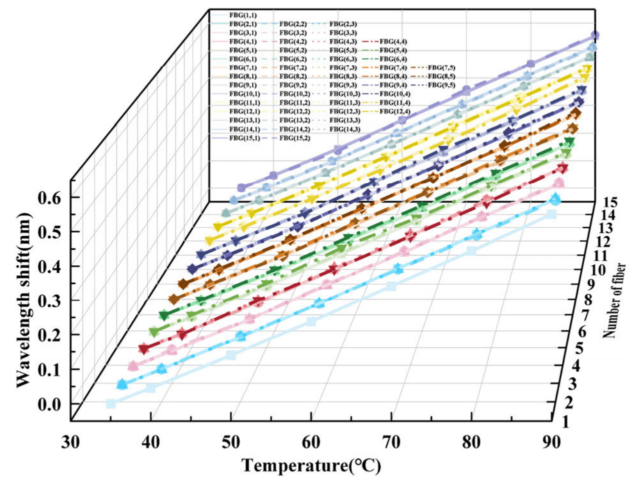

Fig. 6. Sensitivity of the FBG sensors on each optical fiber in the range of 35 °C–90 °C.

TABLE III
KEY SPECIFICATION OF THE EQUIPMENT USED FOR EXPERIMENTS

Equipment	Type	Details
Wire bonder system	MPP iBond5000	Built-in Digital Work Stage Temperature
Thermocouple	Omega TT-T-36	Temperature range: -200°C-260°C Accuracy: ±1.5°C
Demodulator	SN FBGI-16B-3	16 Channel 3Hz Sampling Rate Repeatability: ±1pm
Thermal camera	Fluke Tix580	Temperature Range: -20°C-1000°C Accuracy: ±2°C or 2% Thermal sensitivity (NETD): ≤0.05°C@30°C
Multi-channel thermometer	ApplentInstrument AT4208	8 Channel Thermocouple Temperature Range: 200°C-1300°C Accuracy:0.2%+1°C
PC	HP	Demodulator software

E. Reconstruction of Wafer Surface Temperature Field

FBG sensor can only obtain a point temperature. In this article, for the wafer surface core region and the overall region to design two TMWs, the number of sensors up to 20 and 54, it is still unable to intuitively respond to the temperature distribution of the entire wafer surface, so it is necessary to reconstruct the temperature distribution of the wafer surface through the temperature field reconstruction algorithm from the sparse measurement data. This article

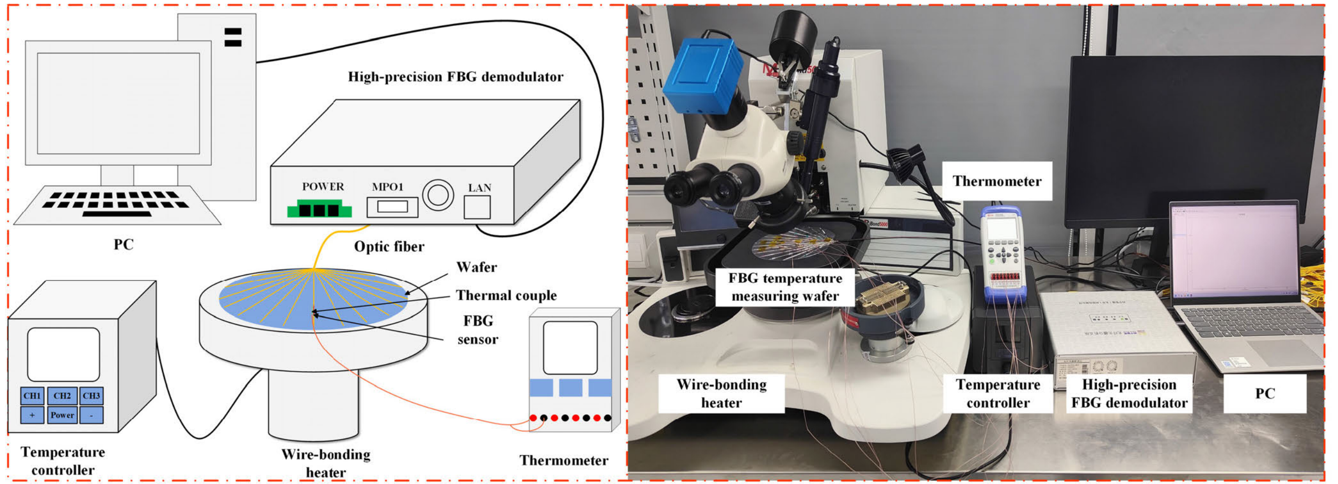

Fig. 7. Schematic of the experimental setup for temperature monitoring using FBG measurement wafer during the wire-bonding process.

TABLE IV
MAXIMUM TEMPERATURE DIFFERENCE FOR EACH FBG WITH THE SAME SENSOR SERIAL NUMBER

FBG serial number	Difference in temperature (℃)
(i,1)	6.301
(i,2)	2.136
(i,3)	1.660
(i,4)	0.426
(i,5)	0.954

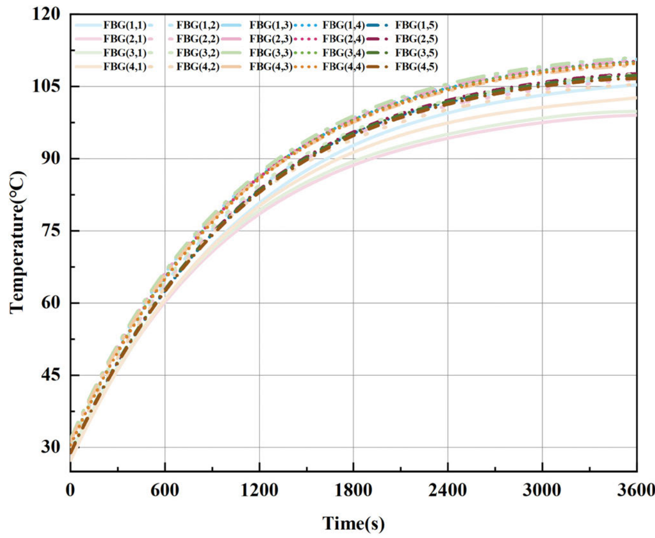

Fig. 8. Thermal behavior of different FBG sensors on the linear-shaped temperature measurement wafer.

uses the Gaussian radial basis function algorithm to reconstruct the wafer surface's temperature field. The radial basis function belongs to the multivariate function, a class of radial distance as a variable set of basis functions for the spatial location and temperature of the two points on the wafer surface. Then, the Euclidean distance between the two points $T_i(x_i, y_i)$ and $T_j(x_j, y_j)$ is

$$R_{(T_i,T_j)} = \sqrt{\left(x_i - x_j\right)^2 + (y_i - y_j)^2} \tag{5}$$

$(x_i, y_i) \in R^n$, $i = 1, 2, \ldots, N$ is a set of discrete points in 2-D space. Corresponding function values are $T_i = f(x_i, y_i) \in R$, $i = 1, 2, \ldots, N$.

The value of the function or any point on the unknown space–temperature function can be expressed as a linear combination of radial basis functions

$$T(x, y) = \sum_{i=1}^{N} \omega_i \phi_i(x, y) \tag{6}$$

where N is the number of interpolation points, ω_i is the coefficient to be determined, and ϕ_i is the radial basis function. This article chooses the Gaussian function as the basis function, which takes the form

$$\phi = e^{-\frac{R^2}{c^2}} \tag{7}$$

where R is the Euclidean distance between two discrete points in 2-D space, and c is the shape parameter of the radial basis function. After the shape parameters are determined, the system of equations is obtained by substituting the temperature data obtained from measurements

$$T = \omega\phi. \tag{8}$$

After solving for the matrix of coefficients to be determined, $T(x, y)$—the value of the temperature function at any point in space—can be approximated by interpolation using Gaussian radial basis functions.

III. RESULTS AND ANALYSIS

The wire bonding system is used to heat the LTMW with a temperature range of 30 °C–110 °C. The demodulator sampling rate is set to 1 Hz, and the heating time is 3600 s. The temperature of the wafer is measured using various sensors, and the results are shown in Fig. 8. The overall trend of the temperature is toward convergence, and the gradient of the temperature rise gradually decreases until it stabilizes. The results of each FBG measurement with the same sensor number were compared, and the maximum temperature difference of FBGs with the same sensor number is shown in

Fig. 9. Comparison between the temperature variation monitored by FBG sensors and Thermal couple sensors. (a) Optical fiber 1. (b) Optical fiber 2. (c) Optical fiber 3. (d) Optical fiber 4.

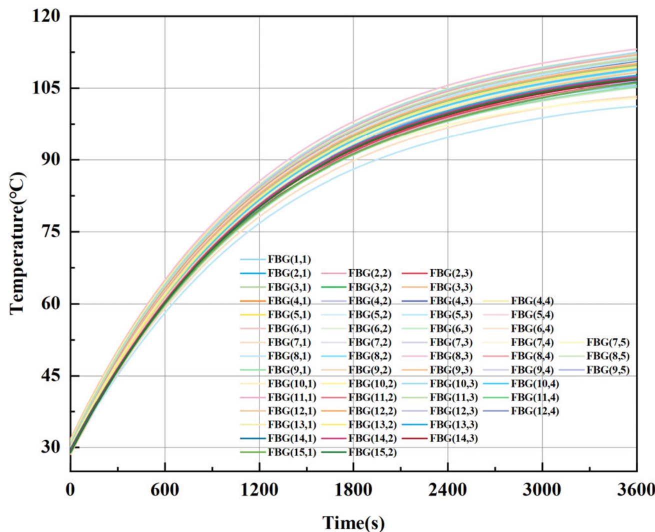

Fig. 10. Thermal behavior of different FBG sensors on the FTMW.

Table IV. The minimum temperature value was obtained from the first FBG on each fiber, and the maximum temperature difference was 6.301 °C, indicating that the lower half of the wafer is near the notch and has a temperature defect region. On the other hand, the temperature difference on the upper half of the wafer is much smaller, and the temperature of the same-numbered FBG tends to be the same, indicating a more uniform temperature distribution in the center of the wafer and the upper half. The results of comparative TC measurements are shown in Fig. 9(a)–(d). The temperature measured by the exact number of FBG is significantly higher than the TC. For example, the maximum temperature difference between the TC and FBG sensor of serial numbers (4,5) is 11.345 °C at 3600 s, and temperatures measured by FBGs are significantly higher than those by TCs. The FBG measurement result is more accurate and closer to the temperature set by the temperature controller of the wire-bonding machine.

To obtain a broader range of wafer surface temperature distribution data, the above experiments are repeated using FTMW, the results of which are shown in Fig. 10. At 3600 s, the lowest temperature on the wafer surface is measured as 101.23 °C for FBG (8,1), which is located at the wafer notch, and the highest temperature was measured as 113.17 °C for FBG (8,3), which is situated in the center of the wafer. The trend is consistent with the measured results of LTMW. Significant temperature differences between sensors are distributed radially across the wafer surface; the highest temperature is

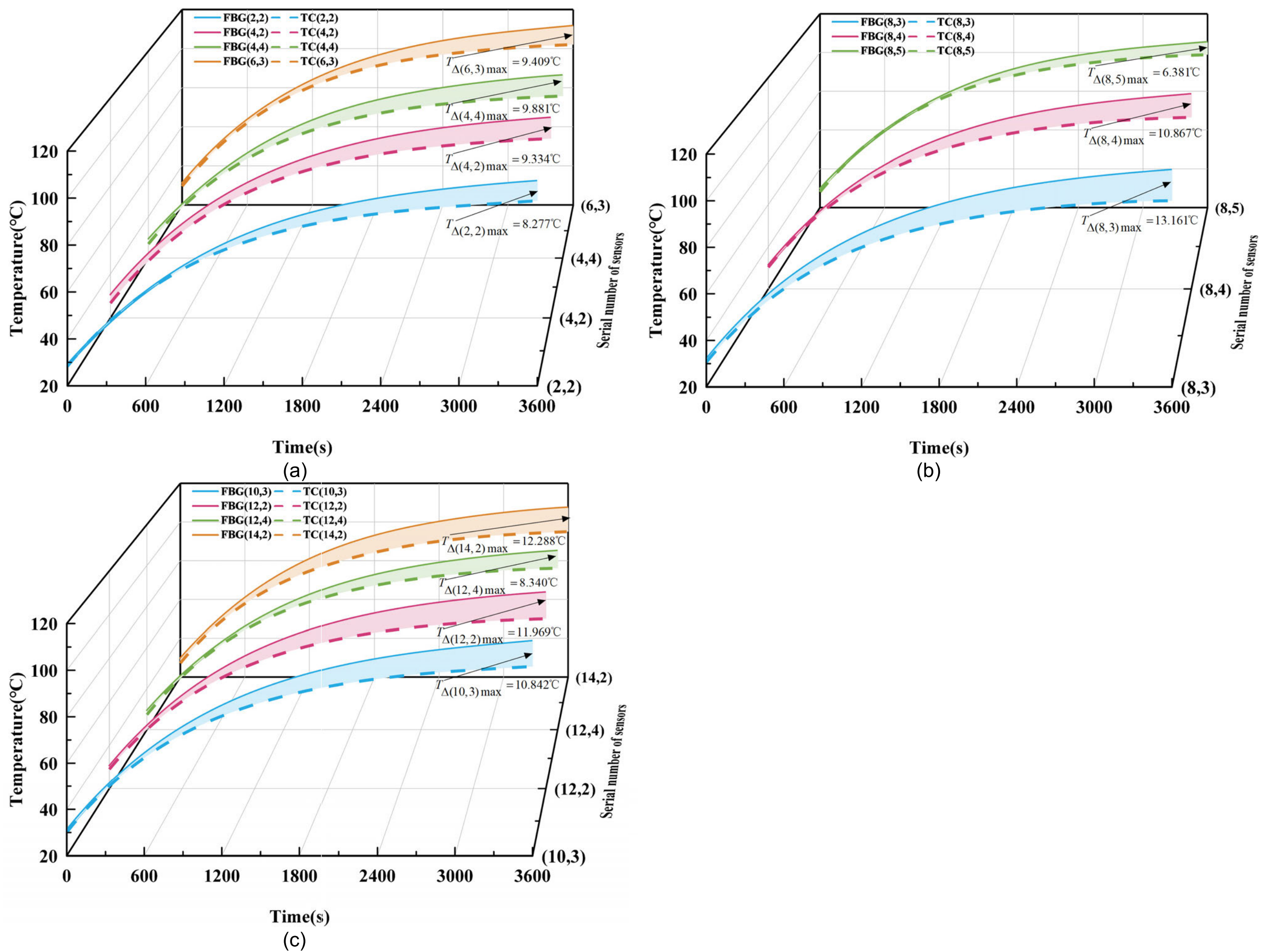

Fig. 11. Comparison between the temperature variation monitored by FBG sensors and Thermal couple sensors. (a) Left part of the wafer. (b) Middle part of the wafer. (c) Right part of the wafer.

in the center of the wafer, and it is gradually reduced to the edge of the wafer.

The maximum temperature difference is 11.94 °C. At the same time, FBG (7,5) for the wafer surface temperature of the second lowest point is 103.27 °C, indicating the temperature defects in this region. Due to the large number of wafer surface temperature FBG sensors, the (2,2) (4,2) (4,4) (6,3) (8,3) (8,4) (8,5) (10,3) (12,2) (12,4) (14,2) FBGs are selected for the comparison with TC measurements, as shown in Fig. 11. The sensors are divided into three regions: left half, center, and right half. The FBG and TC sensors arranged on the left half of the wafer surface find that the maximum temperature difference of 9.881 °C occurs between sensor groups numbered (4,4).

The maximum temperature difference between the (8,3) sensors group is 13.161 °C in the middle region. The maximum temperature difference of the right side of the wafer between the (14,2) sensor group is 12.288 °C. The temperatures obtained from the FBGs are significantly higher than the TCs, and the measurement results are more accurate and closer to the setting of the wire bonding system. The measurement accuracy of the FBG sensor is higher compared to TC. Also, since the FBG sensor is wrapped in polyimide, for being in an open environment at the same time, the TC dissipates more heat, resulting in a more enormous difference in its measurement results compared to the FBG sensor.

The temperature field reconstruction algorithm uses the sparse temperatures obtained from the FBG sensor network distributed on the surface of the FTMW to reconstruct the temperature distribution on the wafer surface. Starting from 0 s, the wafer surface temperature field is reconstructed once in 600 s intervals, and the temperature range is set to 25 °C–120 °C. The results are shown in Fig. 12(c), which shows that the temperature distribution on the wafer surface exhibits a gradual decrease from the center to the edges trend, consistent with the sensors' measurement results. Taking the reconstruction results of the wafer surface temperature field at 3600 s as an example, the upper and lower temperature limits are rescaled to highlight a more specific temperature distribution, and the results are shown in Fig. 12(b), which are compared with the image taken with the infrared thermal imager at the same time offered in Fig. 12(a). There are two thermal defect areas: the notch and the left upper part of the wafer. It indicates that the temperature distribution of the wafer surface shows a gradual decrease from the center to the edges, consistent with the measurement results. This shows that the temperature field reconstruction algorithm can correctly respond to the wafer surface temperature distribution.

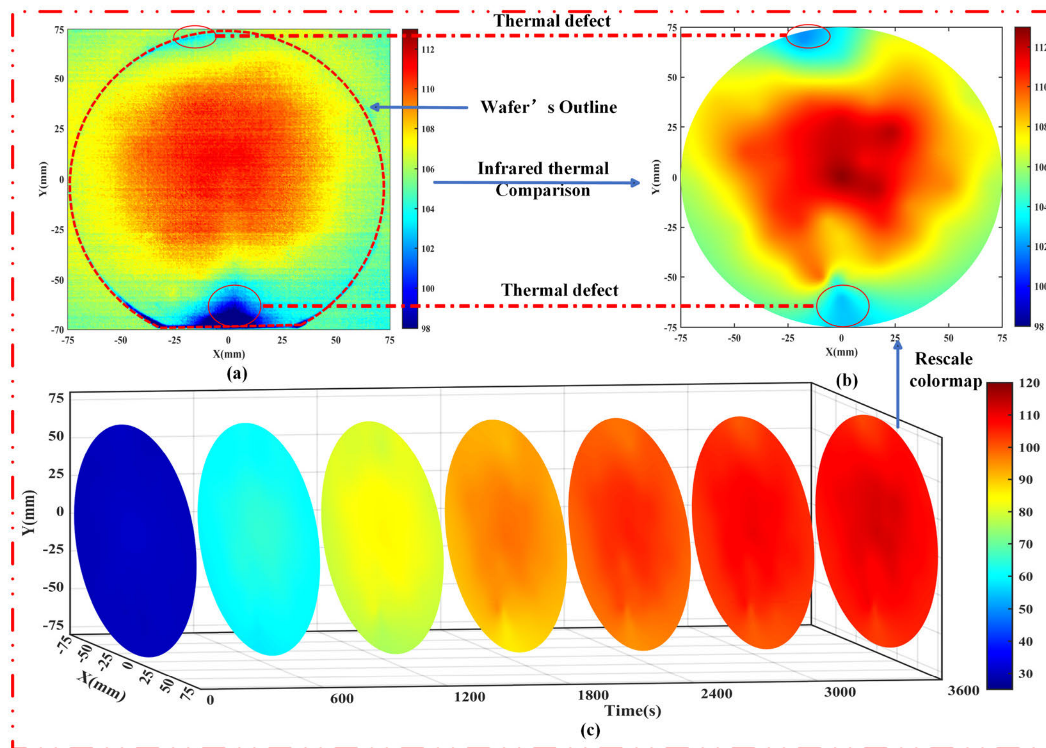

Fig. 12. Temperature field reconstruction results and comparison with the wafer surface thermal image. (a) Wafer surface thermal image. (b) Temperature field distribution on the wafer surface at 3600 s. (c) Temperature field distribution of the whole wire bonding heating process.

IV. Conclusion

To monitor the wafer surface temperature during the MEMS process with high accuracy and to improve the temperature control accuracy of the MEMS process, this article proposes a sensor network of multiple FBGs to monitor the wafer surface temperature distribution during the wire bonding process and reconstruct the wafer surface temperature field distribution based on the measurement point temperature data. For the two TMWs fabricated in this article, heating experiments were conducted from 30 °C to 110 °C. Although the LTMW has the advantage of being easy to manufacture, its coverage area is relatively small. Its temperature field reconstruction accuracy is poor. In order to improve the sensors' coverage on the wafer surface, the FTMW was fabricated, and the sparse temperature point data obtained from the FTMW measurements were utilized to reconstruct the temperature field on the wafer surface and compared with the results of the infrared thermal imager measurements. The results show that a law exists for monitoring the heating process of the wire-bonding machine, namely, the radial distribution of the wafer surface temperature distribution. The maximum temperature difference is 11.94 °C. After comparing it with the thermal imaging camera and TC comparison, it can be seen that the reconstruction of the wafer surface temperature field is better, and it can accurately identify the key areas where the temperature defects occur. Hence, it is a promising method for monitoring the temperature of the wafers.

References

[1] T. Sahoo et al., "Growth of ZnO thin film on p-GaN/sapphire (0001) by simple hydrothermal technique," *J. Cryst. Growth*, vol. 310, no. 3, pp. 570–574, Feb. 2008.

[2] K. Bobzin, T. Brögelmann, and N. C. Kruppe, "Enhanced PVD process control by online substrate temperature measurement," *Surf. Coatings Technol.*, vol. 354, pp. 383–389, Nov. 2018.

[3] R. L. Puurunen and F. Gao, "Influence of ALD temperature on thin film conformality: Investigation with microscopic lateral high-aspect-ratio structures," in *Proc. 14th Int. Baltic Conf. At. Layer Deposition (BALD)*, Oct. 2016, pp. 20–24.

[4] B. Adams, "Temperature measurement in RTP: Past and future," in *Proc. 16th IEEE Int. Conf. Adv. Thermal Process. Semiconductors*, Las Vegas, NV, USA, Sep. 2008, pp. 117–125.

[5] G. Leitz, J. Pezoldt, I. Patzschke, J.-P. Zöllner, and G. Eichhorn, "Investigation of dynamical temperature behaviour in rtp," *MRS Proc.*, vol. 303, p. 171, Aug. 1993.

[6] W. Wan Tan and R. F. Y. Li, "An in-situ temperature measurement system for DUV lithography," *IEEE Trans. Instrum. Meas.*, vol. 52, no. 4, pp. 1136–1142, Aug. 2003.

[7] M. Häffner et al., "Influence of temperature on HSQ electron-beam lithography," *J. Vac. Sci. Technol. B, Microelectron. Nanometer Struct. Process., Meas., Phenomena*, vol. 25, no. 6, pp. 2045–2048, Nov. 2007.

[8] T. Iuchi and T. Seo, "Radiation thermometry of silicon wafers based on emissivity-invariant condition," *Appl. Opt.*, vol. 50, no. 3, pp. 323–328, Jan. 2011.

[9] Y. Yamada, J. Ishii, A. Nakaoka, and Y. Mizojiri, "Silicon wafer surface-temperature monitoring system for plasma etching process," *Int. J. Thermophys.*, vol. 32, nos. 7–8, pp. 1457–1466, Aug. 2011.

[10] T. Ni and M. Barnes, "Rapid IR transmission thermometry for wafer temperature sensing," U.S. Patent 6 062 729, May 16, 2000.

[11] Y. Toyoda, T. Seo, and T. Iuchi, "Non-contact temperature measurement of silicon wafers based on the combined use of transmittance and radiance," *Measurement*, vol. 51, pp. 393–399, May 2014.

[12] Y. Toyoda and T. Iuchi, "Non-contact temperature measurement for silicon wafers under 600 °C," in *Proc. SICE Annu. Conf. (SICE)*, Aug. 2012, pp. 27–31.

[13] T. Iuchi and A. Gogami, "Simultaneous measurement of emissivity and temperature of silicon wafers using a polarization technique," *Measurement*, vol. 43, no. 5, pp. 645–651, Jun. 2010.

[14] C. Koshimizu, T. Ohta, T. Matsudo, S. Tuchitani, and M. Ito, "Low-coherence interferometry-based non-contact temperature monitoring of a silicon wafer and chamber parts during plasma etching," *Appl. Phys. Exp.*, vol. 3, no. 5, Apr. 2010, Art. no. 056201.

[15] T. Tsutsumi, Y. Fuknaga, K. Ishikawa, H. Kondo, M. Sekine, and M. Hori, "Real-time control of a wafer temperature for uniform plasma process," in *Proc. Int. Symp. Semiconductor Manuf. (ISSM)*, Dec. 2018, pp. 1–4.

[16] O. Daniel et al., "In-situ wafer temperature measurement during firing process via inline infrared thermography," in *Proc. AIP Conf.*, Sep. 2019, vol. 2156, no. 1, p. 20013.

[17] V. Patel, M. Patel, S. Ayyagari, W. F. Kosonocky, D. Misra, and B. Singh, "Wafer temperature measurements and end-point detection during plasma etching by thermal imaging," *Appl. Phys. Lett.*, vol. 59, no. 11, pp. 1299–1301, Sep. 1991.

[18] F. Levent Degertekin, J. Pei, B. T. Khuri-Yakub, and K. C. Saraswat, "In situ acoustic temperature tomography of semiconductor wafers," *Appl. Phys. Lett.*, vol. 64, no. 11, pp. 1338–1340, Mar. 1994.

[19] K. G. Kreider and G. Gillen, "High temperature materials for thin-film thermocouples on silicon wafers," *Thin Solid Films*, vol. 376, nos. 1–2, pp. 32–37, Nov. 2000.

[20] K. G. Kreider and F. DiMeo, "Platinum/palladium thin-film thermocouples for temperature measurements on silicon wafers," *Sens. Actuators A, Phys.*, vol. 69, no. 1, pp. 46–52, Jun. 1998.

[21] J. L. Hoyt, K. E. Williams, and J. F. Gibbons, "Method of welding thermocouples to silicon wafers for temperature monitoring in rapid thermal processing," U.S. Patent 4 787 551, Nov. 29, 1988.

[22] Z. Li et al., "Effect of thermocouple position on temperature field in nitride MOCVD reactor," *J. Cryst. Growth*, vol. 368, pp. 29–34, Apr. 2013.

[23] A. M. van Graven and R. A. M. Wolters, "Wafer temperature measurement in PVD systems using the Co-Si reaction," *Microelectron. Eng.*, vol. 50, nos. 1–4, pp. 495–499, Jan. 2000.

[24] M. C. Chuang and J. C. Huang, "Wafer temperature sensing methods and related semiconductor wafer," U.S. Patent 9 562 943, Feb. 7, 2017.

[25] J. Engelmann et al., "Measuring the wafer temperature in CVD tools using the wireless sensarray hightemp-400 wafer," in *Proc. 28th Annu. SEMI Adv. Semiconductor Manuf. Conf. (ASMC)*, Saratoga Springs, NY, USA, May 2017, pp. 161–164.

[26] L. Zhang et al., "Real-time battery temperature monitoring using FBG sensors: A data-driven calibration method," *IEEE Sensors J.*, vol. 22, no. 19, pp. 18639–18648, Oct. 2022.

[27] J. Peng, S. Jia, H. Yu, X. Kang, S. Yang, and S. Xu, "Design and experiment of FBG sensors for temperature monitoring on external electrode of lithium-ion batteries," *IEEE Sensors J.*, vol. 21, no. 4, pp. 4628–4634, Feb. 2021.

[28] F. Huang et al., "Real-time monitoring of temperature field distribution of three-element LiB lithium battery using FBG arrays," *IEEE Sensors J.*, vol. 23, no. 24, pp. 30473–30480, Dec. 2023.

[29] H. Ren et al., "Quasi-distributed temperature detection of press-pack IGBT power module using FBG sensing," *IEEE J. Emerg. Sel. Topics Power Electron.*, vol. 10, no. 5, pp. 4981–4992, Oct. 2022.

[30] S. Chen, D. Vilchis-Rodriguez, S. Djurovic, M. Barnes, P. Mckeever, and C. Jia, "Direct on chip thermal measurement in IGBT modules using FBG technology—Sensing head interfacing," *IEEE Sensors J.*, vol. 22, no. 2, pp. 1309–1320, Jan. 2022.

[31] S. Chen, D. Vilchis-Rodriguez, S. Djurovic, M. Barnes, P. McKeever, and C. Jia, "FBG head size influence on localized on-chip thermal measurement in IGBT power modules," *IEEE Sensors J.*, vol. 22, no. 22, pp. 21684–21693, Nov. 2022.

[32] C. Wei-Gen, L. Jun, W. You-Yuan, L. Liu-Ming, Z. Jian-Bao, and Y. Yan-Feng, "The measuring method for internal temperature of power transformer based on FBG sensors," in *Proc. Int. Conf. High Voltage Eng. Appl.*, Chongqing, China, Nov. 2008, pp. 672–676.

[33] G. G. Kuhn, K. M. Sousa, C. Martelli, C. A. Bavastri, and J. C. C. da Silva, "Embedded FBG sensors in carbon fiber for vibration and temperature measurement in power transformer iron core," *IEEE Sensors J.*, vol. 20, no. 22, pp. 13403–13410, Nov. 2020.

[34] A. Leal-Junior et al., "Fiber Bragg gratings in CYTOP fibers embedded in a 3D-printed flexible support for assessment of human–robot interaction forces," *Materials*, vol. 11, no. 11, p. 2305, Nov. 2018.

[35] C. A. F. Marques et al., "Aviation fuel gauging sensor utilizing multiple diaphragm sensors incorporating polymer optical fiber Bragg gratings," *IEEE Sensors J.*, vol. 16, no. 15, pp. 6122–6129, Aug. 2016.

[36] G. Lopes et al., "Innovative optical pH sensors for the aquaculture sector: Comprehensive characterization of a cost-effective solution," *Opt. Laser Technol.*, vol. 171, Apr. 2024, Art. no. 110355.

[37] V. Mishra, M. Lohar, and A. Amphawan, "Improvement in temperature sensitivity of FBG by coating of different materials," *Optik*, vol. 127, no. 2, pp. 825–828, Jan. 2016.

[38] C. Marques et al., "Advances on polymer optical fiber gratings using a KrF pulsed laser system operating at 248 nm," *Fibers*, vol. 6, no. 1, p. 13, Mar. 2018.

[39] C. A. F. Marques, L. B. Bilro, N. J. Alberto, D. J. Webb, and R. N. Nogueira, "Narrow bandwidth Bragg gratings imprinted in polymer optical fibers for different spectral windows," *Opt. Commun.*, vol. 307, pp. 57–61, Oct. 2013.

[40] C. A. F. Marques et al., "Fast and stable gratings inscription in POFs made of different materials with pulsed 248 nm KrF laser," *Opt. Exp.*, vol. 26, no. 2, pp. 2013–2022, Jan. 2018.

Yuhao Feng is currently pursuing the master's degree with the School of Instrument and Opto-Electronics Engineering, Beijing Information Science and Technology University, Beijing, China.

His current research mainly focuses on instrument technology, photoelectric measurement, and multisource information fusion.

Jingjing Peng received the B.S. degree from Central South University, Changsha, China, in 2012, and the Ph.D. degree from Tsinghua University, Beijing, China, in 2017.

She is an Assistant Research Fellow at the State Key Laboratory of Precision Measurement Technology and Instruments, Tsinghua University. Her research focuses on the test technology of intelligent integrated microsystems.

Tao Wu received the B.S. degree from Lanzhou University, Lanzhou, China, in 2019, and the master's degree from the Institute of Electronic Engineering, China Academy of Engineering Physics (CAEP), Mianyang, China, in 2021.

His current research mainly focuses on micropower and online measurement technology.

Fei Xing received the B.S. degree from Tongji University, Shanghai, China, in 2002, and the Ph.D. degree in instrument science and technology from Tsinghua University, Beijing, China, in 2006.

He is currently a Professor with Tsinghua University. His current research mainly focuses on instrument technology, photoelectric measurement, and multisource information fusion.

Ting Sun received the B.S. degree from Tianjin University, Tianjin, China, in 2009, and the Ph.D. degree in instrument science and technology from Tsinghua University, Beijing, China, in 2014.

Since 2016, she has been an Associate Professor with Beijing Information Science and Technology University, Beijing. Her main research interests include instrument technology, photoelectric measurement, and multisource information fusion.